ASM Sc. J., 16, 2021

https://doi.org/10.32802/asmscj.2021.776

Ni(II) Butylmethyldithiocarbamate: Physico-Chemical Properties, X-Ray Crystallography, DFT and Anti-Corrosion Screening in Different Acids

Nor Farah Hida Othman[1], Noor Syafiqah Habdul Latif[1], Sheikh Ahmad Izaddin Sheikh Mohd Ghazali[1], Erna Normaya Abdullah[2] and Nur Nadia Dzulkifli[1*]

[1]*Faculty of Applied Sciences, University Teknologi MARA, Cawangan Negeri Sembilan, Kampus Kuala Pilah 72000, Kuala Pilah, Negeri Sembilan, Malaysia*

[2]*Experimental and Theoretical Research Laboratory, Department of Chemistry, International Islamic University Malaysia, Bandar Indera Mahkota, 25200 Kuantan, Pahang, Malaysia*

In industrial sectors, pickling and acid cleaning are mutual processes where acid solutions, such as hydrochloric acid (HCl) and sulfuric acid (H_2SO_4), are used to eliminate the corrosion products yielded on metal surfaces; thus, improving the performance of the machineries. However, the usage of the acid could lead to another metal deterioration. Dithiocarbamate inhibitor is defined as an organic compound that has good corrosion inhibition properties that can work as an inhibitor in an acid environment. Dithiocarbamate (DTC) assists by reducing acid reactiveness which prohibits metal dissolution in the acid. In this study, the Ni(II) *N*-butylmethyldithiocarbamate (Ni[BuMedtc]$_2$) complex was synthesised by using an in-situ method and characterised by elemental analyser, attenuated total reflection Fourier transform infrared (ATR-FTIR), ultraviolet-visible (UV-Vis) spectroscopy and X-ray crystallographic study, and the chemical properties of the Ni[BuMedtc]$_2$ complex was successfully calculated by the Discrete Fourier Transform (DFT) approach. The experimental results which were obtained through the weight-loss analysis method in two different acids – 1 M HCl and 1 M H_2SO_4 – indicated that the inhibition efficiency increased as the inhibitor concentration increased. The outcome showed that the Ni[BuMedtc]$_2$ performed better as an inhibitor in 1 M HCl as compared to in1 M H_2SO_4 to protect the metal exterior because H_2SO_4 is more corrosive due to the excessive presence of H^+.

Keywords: corrosion inhibitor; concentration; dithiocarbamate

I. INTRODUCTION

Corrosion is a condition where a metal undergoes deterioration and loses its critical possessions due to chemical, electrochemical and other reactions of the exposed surface. Extreme corrosion occurs especially during the cleaning process when corrosive acids are used. Increasing economic loss due to metal corrosion is a major concern in the industrial sector. A convenient approach to address the problem of metal corrosion is by the application of organic corrosion inhibitors. Furthermore, to use organic corrosion inhibitors is the most effective and economical method among all anticorrosive ways (Qiang *et al.,* 201). Corrosion inhibitor plays an important role in handling industrial metal corrosions. It can prevent metal dissolution and reduce acid consumption (Soltani *et al.,* 2016). As reported, various types of organic compounds act as corrosion inhibitors and contain multiple bonds in their structures that mainly contain nitrogen (N), sulfur (S) or oxygen (O) atoms (Hong-bo *et. al.,* 2002, Hebbar *et al.,* 2014). High electron density on the heteroatoms, such as N, O, and S, has a high tendency to resist corrosion due to the

*Corresponding author's e-mail: nurnadia@uitm.edu.my

strong tendency of N and S to share electrons with metal to form ring chelates (Liu *et al.,* 2019). Figure 1 shows the general structure of DTC. In recent years, DTC complex is widely applied in various areas, such as manufacturing, agricultural and biological activities (Kanchi *et. al.,* 2014; Szolar, 2007). DTC is known as a versatile ligand due to its ability to form complexes with almost all elements and stabilise a variety of oxidation states of transition metals (Kamaludin *et. al.,* 2013; Nabipour *et al.,* 2010). Dithiocarbamates are characterised with the partial double bond character of C-N and C-S of thioureide moiety (Andrew & Ajibade 2018). In this study, the synthesis and characterisation of Ni[BuMedtc]$_2$ complex was investigated to evaluate the complex's potency as a corrosion inhibitor, whereas the chemical properties of the Ni[BuMedtc]$_2$ complex calculated by DFT method was evaluated.

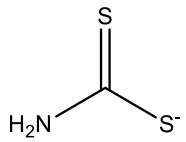

Figure 1. The structure of DTC

II. MATERIALS AND METHODS

A. Material and Physical Measurement

The chemicals used were purchased from Sigma Aldrich and used without purification. The melting point was determined in capillary tube by using a melting point apparatus, namely the SMP10 Stuart model. Elemental analysis of carbon (C), hydrogen (H), nitrogen (N) and sulfur (S) of the Ni[BuMedtc]$_2$ complex was carried out with Elemental Fison EA 1108 CHNS-O analyser. The FTIR-ATR spectra were recorded on ATR plate disc by using Perkin Elmer model GX spectrophotometer in the range of 4000-650 cm^{-1} at room temperature. The electronic spectra were measured by PG instrument T80/T80+ spectrophotometer in the region of 200-600 nm by using DMSO as a solvent. Gravimetric analysis was done by using a Lindberg/Blue furnace with temperatures that ranged from room temperature to 600°C. Molar conductivity value was measured at room temperature by using SI Analytic Lab 970 conductivity meter at the concentration of 2 x 10^{-3} M with DMF as a solvent. X-ray crystallography study was executed on a Bruker Apex II CCD diffractometer at 0 K. The structure and bonding properties of the Ni[BuMedtc]$_2$ complex were studied by using DFT calculations.

B. Synthesis of Ni[BuMedtc]$_2$ Complex

Ni[BuMedtc]$_2$ complex was synthesised by using in-situ method at 277 K in ethanol. 2 mmol carbon disulfide (CS_2) was added into 3 mmol *N*-butylmethylamine and stirred for 1 h. Next, 1 mmol Ni(II) nitrate solution was added dropwise into the mixture and continued with another 1 h of stirring to obtain a green precipitate. The precipitate was then filtered and washed by using ethanol and dried in a desiccator. The recrystallisation of the product was done in the mixture of ethanol and chloroform with a ratio of 1:3.

C. Recrystallisation and X-ray Crystallography Study

Recrystallisation process was carried out by dissolving the complex in ethanol (EtOH) and chloroform (1:3 v/v). The crystallographic study was collected by the detector diffractometer (Mo K= 0.71076 Å) on a crystal with a size range of $3.046 < \theta < 25.095$.

D. Weight Loss Measurements

Mild steel specimens of (2 x 3.5) cm^2 in dimensions were polished by using an emery paper and washed with distilled water, followed with acetone and then dried at room temperature. The specimens were weighed before and after the immersion in 10 mL of 1M HCl and H_2SO_4 for 24 h in the absence and presence of various concentrations of the inhibitor at 40 °C. The percentage inhibition efficiency was calculated by:

$$\%\,\eta w = \frac{W1\,W2}{s\,t}\,x100$$

Where, W_1 and W_2 are the weight loss in the absence and presence of the inhibitor, respectively, s is the surface area of the mild steel and t is the time taken.

E. Computational Method

The crystal was optimised in the solution phase using a continuum solvent model (CPCM) based on density functional theory (DFT) at the B3LYP/LANL2DZ level before it was further used to calculate chemical reactivity properties (Latif *et al*., 2018).

III. RESULTS AND DISCUSSION

A. Physical Properties of Ni[BuMedtc]₂ Complex

The Ni[BuMedtc]$_2$ complex was prepared by using in-situ technique with the ratio of 2:2:1 (CS_2: amine: Ni(II) salt). The yield of the synthesised complex was high, which was 75% for Ni[BuMedtc]$_2$. The general reaction scheme of the Ni[BuMedtc]$_2$ complex preparation is shown in Figure 2. The colour of the complex was observed as dark green for Ni[BuMedtc]$_2$ and was stable at an open atmosphere as well as soluble in dimethylsulfoxide (DMSO), ethanol (EtOH), methanol (MeOH) and tetrahydrofuran (THF), but partially soluble in water (H_2O). The melting point for the Ni[BuMedtc]$_2$ complex was higher than 300°C, which occurred due to the formation of covalent bonds in the metal complexes. Meanwhile, the molar conductivity for Ni[BuMedtc]$_2$ revealed that the complex was a non-electrolyte since the value appeared in the range of 0-30 S cm^2 mol^{-1}. The CHNS elemental analysis data showed congruence between the experimental and theoretical values based on the suggested general structures. Table 1 shows the physical properties of Ni[BuMedtc]$_2$.

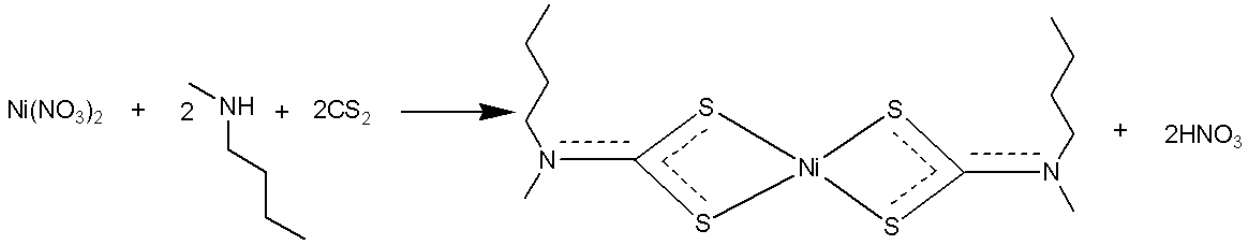

Figure 2. The general reaction scheme of the Ni[BuMedtc]$_2$ complex

Table 1. Physical characteristics of synthesised inhibitor

Complex	Colour	Yield (%)	MP	MC (S cm² mol⁻¹)	Elemental analysis (calculated)			
					C	H	N	S
Ni[BuMedtc]$_2$	Dark green	75	> 300	2.0	37.60 (37.20)	6.30 (6.44)	7.30 (7.68)	33.46 (33.15)

*( ) = calculated value
*MP = melting point
*MC = Molar conductivity

B. IR Spectra

The contrast of vital stretching bands that were obtained from FTIR-ATR spectrophotometer for CS_2, *N*-butylethylamine and Ni[BuMedtc]$_2$ are shown in Figure 3 and listed in Table 2. The Ni[BuMedtc]$_2$ complex showed an appearance of a strong absorption band at 1518 cm^{-1}, which indicated the presence of ν(C⋯N) band, whereas CS_2 and *N*-butylethylamine did not contain the absorption. This band is known as a thioureide band which is shown by the partial double bond character that occurred due to the delocalisation of electron density within the DTC moiety. The ν(C⋯N) band was a derivative of ν(C-N) band in which only *N*-butylethylamine that had the absorption recorded at 1498 cm^{-1}. The shifting in the thioureide value to a higher wavenumber compared with its raw materials was due to the mesomeric drift of π electron density from the dithiocarbamate ligand moiety towards the Ni that increased in carbon-nitrogen double bond character (Sathiyaraj *et al.,* 2018). The outcome was consistent with a

higher character of double bond between the carbon and nitrogen atom (Antonio *et al.,* 2020). The absorption of *ν*(C=S) band shown in CS_2 was at 1541 cm^{-1}. Meanwhile, a medium stretching band that was detected in the region of 967 cm^{-1} for the Ni[BuMedtc]$_2$ complex indicated the presence of *ν*(C⎓S) band. The ν(C–S) band which appeared around 967 cm^{-1} directed a symmetrically bidentate coordination of the $–CS_2$ group to the Ni metal (Bobinihi *et al.,* 2018). The coordination of ligand to the metal centre was verified, whereby the stretching band shifted to a lower wavenumber due to the reduction of the carbon-sulfur double bond character to partial double bond character. The absorption of *ν*(C⎓S) band of the Ni [BuMedtc]$_2$ complex showed a greater character of single bond between the carbon and sulfur atoms in the CS2 group upon complexation. By calculating the number of the splitting of this band, the chelating character of the dithiocarbamate ligand in the complex can be identified (Awang *et al.,* 2010). Based on the results obtained, the Ni[BuMedtc]$_2$ complex possessed a bidentate manner of DTC ligand since there was only a single band present within the region. The absence of ν(N-H) band in the Ni[BuMedtc]$_2$ complex proved that the deprotonation of 2° amines and also proved that coordination occurred between DTC and metal ion.

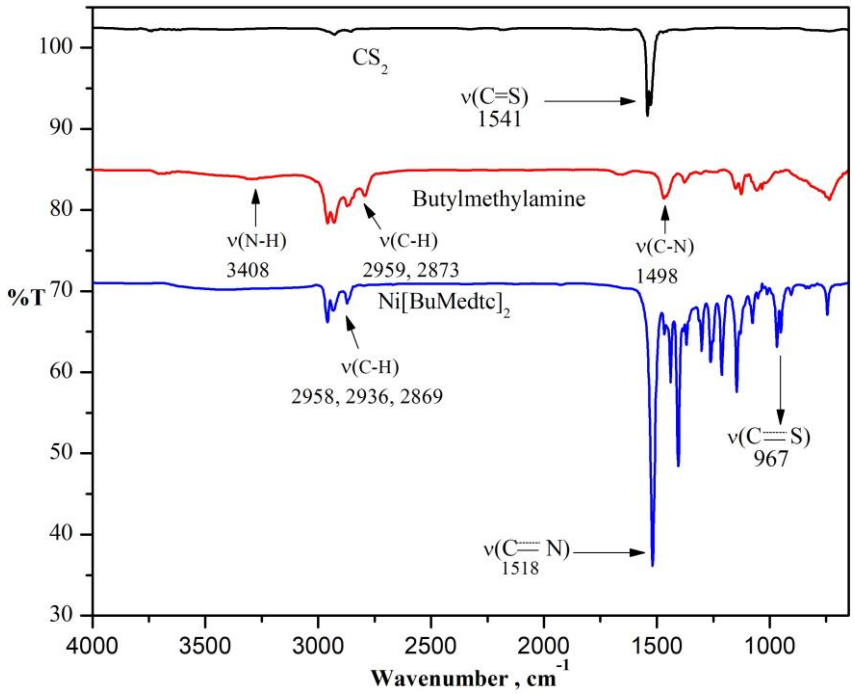

Figure 3. IR spectra of CS_2, *N*-butylethylamine and Ni[BuMedtc]$_2$

Table 2. IR spectra data for CS_2, *N*-butylethylamine and Ni[BuMedtc]$_2$

Compound	**Wavenumber, cm^{-1}**					
	***ν*(C-H)**	***ν*(N-H)**	***ν*(C=S)**	***ν*(C⎓S)**	***ν*(C-N)**	***ν*(C⎓N)**
Carbon disulphide, CS_2	-	-	1541	-	-	-
N-butylethylamine	2959,2873	3408	-	-	1498	-
Ni[BuMedtc]$_2$	2958, 2936,2869	-	-	967	-	1518

C. Electronic Spectra

The structure of Ni[BuMedtc]$_2$ complex can be confirmed by comparing the electronic spectra between the raw materials and the complex as shown in Figure 4. Onwudiwe *et al.* (2016) reported that intra-ligand bands between 205 nm and 280 nm were identified as n-σ* transition (Onwudiwe *et al.,* 2016). The Ni[BuMedtc]$_2$ did not show the n-σ* transition while the CS_2 and *N*-butylethylamine displayed the transition at 235 nm and 241 nm, respectively. The Ni[BuMedtc]$_2$ spectrum exhibited three distinctive absorption peaks at 325 nm, 380 nm and >400 nm. CS_2 did not contain any transition of π-π*, but for *N*-butylethylamine, the transition appeared at 318 nm. The peak appeared at 325 nm for Ni[BuMedtc]$_2$, attributed to the π-π* that moved upward with lower absorbance and had the probability to overlap with n-π* transition. CS_2 and *N*-butylethylamine did not possess any *d-d* transition. In Ni[BuMedtc]$_2$ complex, the *d-d* transition was observed as a weak or small absorption peak at above 400 nm because the transition was categorised as a Laporte Forbidden transition. The electronic spectrum of the complex portrayed a weak absorption peak due to *d-d* transition representing a four-coordinated DTC ligand around the Ni(II) ion.

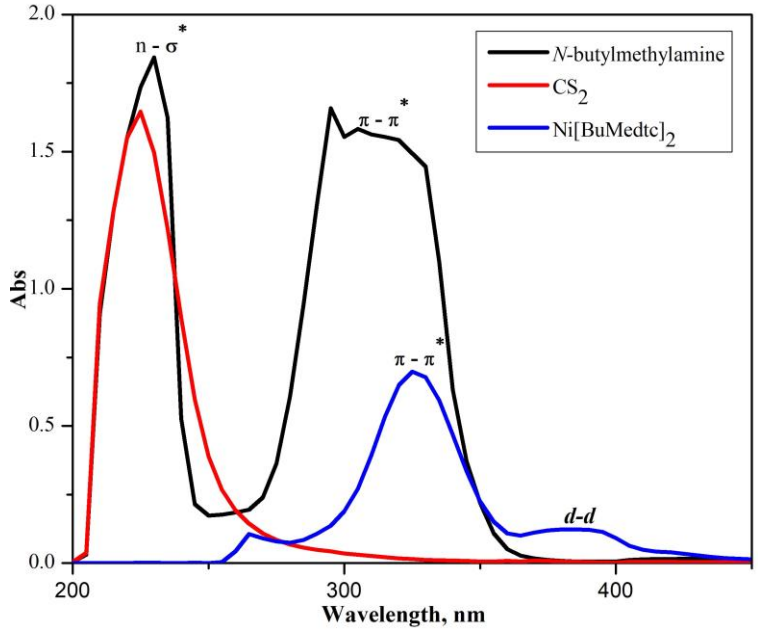

Figure 4. Electronic spectrum of 1.0 x 10^{-5} M of CS_2, *N*-butylethylamine and Ni[BuMedtc]$_2$

D. X-ray Crystallographic Study

From the recrystallisation result, it was proven that Ni[BuMedtc]$_2$ yielded a single crystal structure. Figure 5 shows the ORTEP plot for Ni[BuMedtc]$_2$. Figure 5 reveals that the Ni[BuMedtc]$_2$ complex was a four-coordinated compound in which Ni(II) ion was coordinated to the DTC ligand through thiolate S ion in a bidentate fashion. Ni[BuMedtc]$_2$ adopted a trigonal system with a space group of R-3 and unit cell; where a = 25.544(10) Å, b = 25.544(10) Å, c = 7.018(5) Å, and Z = 9 (Table 3). Figure 5 shows the 3D structure of Ni[BuMedtc]$_2$. From Table 4, the bond length of C-S (1.7144 Å) was between the range of C-S single bond (1.732(3) Å) and C=S double-bond (1.663(3) Å) (Keter *et al.,* 2014). This proved that there was a presence of partial double-bond character in Ni[BuMedtc]$_2$. Meanwhile, the bond length of C-N (1.3113 Å) was shorter as compared to the normal bond length (1.45 Å), which showed the partial double-bond character in this complex. The values of these bond lengths were designated for both C–S and N–C bonds, and alteration of dithiocarbamate with thioureide tautomers in the solid state (El-Sayed *et al.,* 2019). Both bond lengths were in excellent agreement with the ν(C-N) and ν(C-S) stretching bands, as observed in the IR spectra. Ni(II) dithiocarbamate complexes can be found in two types of

geometries, which are tetrahedral and square planar (Beyramabadi *et al.,* 2012). The X-ray Crystallography structure of Ni[BuMedtc]$_2$ showed that it adopted a distorted tetrahedral geometry since two four-membered coordinated rings (S(1)-Ni(1)-S(2) = 79.17° and S(1)-Ni(1)-S(2) = 79.17° were perpendicular to each other. Meanwhile, the distortion of Ni atom of 100.83° was slightly different from the ideal tetrahedral geometry, which was 109.5° and proved that Ni[BuMedtc]$_2$ belonged to distorted tetrahedral geometry. Table 5 shows the bond angle (°) of Ni[BuMedtc]$_2$.

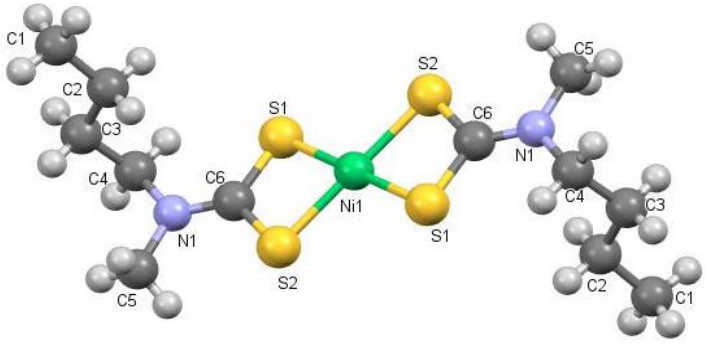

Figure 5. ORTEP plot of Ni[BuMedtc]$_2$ at the 50% probability level with the atom numbering scheme

Table 3. Crystallographic study of Ni[BuMedtc]$_2$

	Ni[BuMedtc]$_2$
Empirical formula	$C_{12}H_{24}N_2NiS_4$
Formula weight (g/mol)	383.30
Crystal system	Trigonal
Space group	R-3
a (Å)	25.544 (10)
b (Å)	25.544 (10)
c (Å)	7.018 (5)
α (°)	90
β (°)	90
γ (°)	120
V (Å^3)	3965 (13)
Mo K (Å)	0.71076
Z	9
D/ Mgm^{-3}	1.445 (5)
F (000)	1818
Color	Green
Temperature	293(2)
Theta range (°)	3.046-25.095
Goodness of fit on F^2	1.064
R indices (all data)	0.0650

Table 4. Bond length (Å) of Ni[BuMedtc]$_2$

Type of bond	Bond length (Å)	Type of bond	Bond length (Å)
Ni(1) - S(1)	2.1952	C(1) - H(1A)	0.96
S(1) - C(6)	1.7118	C(2) - H(2B)	0.97
N(1) - C(6)	1.3113	C(4) - H(4B)	0.97
Ni(1) - S(2)	2.2016	C(1) - H(1B)	0.96
S(2) - C(6)	1.7144	C(3) - H(3A)	0.97
C(1) - C(2)	1.4931	C(5) - H(5A)	0.96
Ni(1) - S(1)a	2.1952	C(1) - H(1C)	0.96
N(1) - C(4)	1.4600	C(3) - H(3B)	0.97
C(2) - C(3)	1.4792	C(5) - H(5B)	0.96
Ni(1) - S(2)a	2.2016	C(2) - H(2A)	0.97
N(1) - C(5)	1.4635	C(4) - H(4A)	0.97
C(3) - C(4)	1.4993	C(5) - H(5C)	0.96

Table 5. Bond angle (°) of Ni[BuMedtc]$_2$

Type of bond	Bond angle (°)	Type of bonding	Bond angle (°)
S(1) - Ni(1) - S(2)	79.17	Ni(1) - S(2) - C(6)	85.20
S(2) - Ni(1) - S(1)a	100.83	C(5) - N(1) - C(6)	120.58
Ni(1) - S(1) - C(6)	85.46	N(1) - C(4) - C(3)	113.47
C(4) - N(1) - C(6)	122.61	S(2) - C(6) - N(1)	124.50
C(2) - C(3) - C(4)	112.99	S(1) - Ni(1) - S(2)a	100.83
S(1) - C(6) - N(1)	125.78	S(1)a - Ni(1) - S(2)a	79.17
S(1) - Ni(1) - S(1)a	180.00	C(4) - N(1) - C(5)	116.77
S(2) - Ni(1) - S(2)a	180.00	C(1) - C(2) - C(3)	114.53
S(1) - C(6) - S(2)	109.71		

E. Molecular Electrostatic Potential

Molecular electrostatic potential (MEP) is commonly used to display the reactivity region of a compound. The MEP mapping of the Ni[BuMedtc]$_2$ complex in Figure 6 shows the appearance of four regions, which were red, yellow, green and blue. The red region at the centre of the compound showed that it contained the highest electron density. This region was categorised as an electrophilic attack region. This effect came from the four electronegative sulfur atoms bonded to the Ni atom to form the Ni[BuMedtc]$_2$ complex.

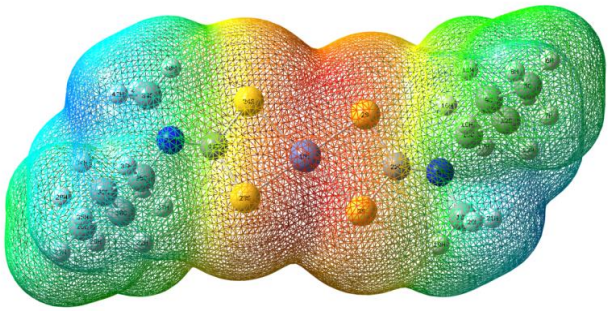

Figure 6. The molecular electrostatic potential (MEP) of the Ni[BuMedtc]$_2$

F. Chemical Reactivity Properties

Table 6 shows the energy value of the chemical reactivity of the Ni[BuMedtc]$_2$. It can be seen that the formation energy of the Ni[BuMedtc]$_2$ was in negative value (-21511.99 eV), showing that the complex was thermodynamically stable. The inertness and stability were also related to the ionisation energy and affinity electron of the compound. In this study, the Ni[BuMedtc]$_2$ showed that its ionisation energy and electron affinity were 5.95 and 1.94 eV, respectively. The calculated result indicated that it aligned with the weight loss data which found that the Ni[BuMedtc]$_2$ was less effective as a corrosion inhibitor due to its stability (Parveen *et al.,* 2016). The calculated data also aligned with the Weight Loss data which showed that the Ni[BuMedtc]$_2$ complex contributed to a significant ability to be a corrosion inhibitor to the mild steel.

Table 6. The calculated reactivity properties of Ni[BuMedtc]$_2$

	Value (eV)
Formation Energy	-21511.99
Ionisation Energy	5.95
Electron affinity	1.94

G. Weight Loss Method

By using the weight loss method, the inhibition efficiency (% η_w) and corrosion rate (C_{RW}) of Ni[BuMedtc]$_2$ were calculated by using the formula equation below:

$$\Delta W = W_1 - W_2 \quad (1)$$

$$C_{RW} = \frac{\Delta W}{s \times t} \quad (2)$$

$$\theta = \frac{C^{\circ}_{RW} - C_{RW}}{C^{\circ}_{RW}} \quad (3)$$

$$\eta_w = \frac{C^{\circ}_{RW} - C_{RW}}{C^{\circ}_{RW}} \times 100\% \quad (4)$$

Where:

W_1 = The initial weight of mild steel before immersion (g).

W_2 = The final weight of mild steel after immersion (g).

ΔW = The weight loss (g).

S = The surface area of the mild steel (cm).

T = Time of immersion (h).

C_{RW} = The corrosion rate in the presence of inhibitor (g cm-2 h-1).

C°_{RW} = The corrosion rate in the absence of inhibitor (g cm-2 h-1).

η_w = The percentage of inhibitor efficiency (%).

The weight loss of mild steel in two types of acids, which were HCI and H_2SO_4, was measured and tabulated in Table 7. It was done to identify the ability of the complex as a corrosion inhibitor. From Table 7, it is displayed that the corrosion rate (C_{RW}) of mild steel decreased as the concentration of inhibitor increased. Meanwhile, the inhibitor efficiency (η_w (%)) increased as the concentration of inhibitor increased. This occurred due to the presence of lone pairs of nitrogen and sulfur atoms in the complex which allowed it to be adsorbed on the metal surface more easily and forming an insoluble stable form on the surface of mild steel which would then reduce the corrosion attack (Noor Khadijah *et. al.,* 2014; Shetty & Shetty 2008). From Figure 7, it can be observed that the complex was able to act as a corrosion inhibitor in different concentrations and types of acid. This was because the complex contained sulfur and nitrogen atoms. The organic compound that had two atoms, which were sulfur and nitrogen, was known as an acid inhibitor. It can be concluded that the inhibitor efficiency increased as the inhibitor concentration increased. In addition, it showed that Ni[BuMedtc]$_2$ can act as an inhibitor better in 1 M HCl than in 1M H_2SO_4. Figure 8 shows the graph of corrosion rate versus inhibitor concentrations of 1 M HCl and 1 M H_2SO_4 in Ni[BuMedtc]$_2$. The graph shows that as the inhibitor concentration was increased, the corrosion rate was gradually decreased and that the corrosion rate in H_2SO_4 was greater than in HCl. The corrosion rate in 1 M H_2SO_4 was higher due to the presence of high concentrations of H^+ in H_2SO_4 which made it more corrosive as compared to HCl (Samina *et al.,* 2011). H_2SO_4 is an effective protonating agent. It can entirely dissociate to form two H^+ ions and enhance the corrosion rate. H_2SO_4 is highly corrosive as emphasised by its highly exothermic (heat generating) reaction with water (Hagen & Jarnberg, 2019). Electrons from the mild steel can react with hydrogen ions in H_2SO_4 acid solutions to form a metal sulfate and produce hydrogen gas which is then adsorbed on

the mild steel surface. The sulfate ions that are integral to sulfuric acid do not participate directly in the corrosion attack. Hydrogen gas can be a problem with mild steel in sulfuric acid environments because it can scrub off the zinc sulfate film which shields the mild steel from acidic attack. This reaction leads to the corrosion of mild steel.

Table 7. Corrosion inhibition data of the Ni[BuMedtc]$_2$ complex in 1 M HCl and H_2SO_4

Acid solution	Complexes	Concentration (M)	Weight loss, ΔW (g)	Corrosion rate, C_{RW} (g cm^{-1} h^{-1})	Inhibitor efficiency, η_w (%)
HCI	Blank	1	0.1630	1.306 x 10^{-3}	-
	Ni[BuMedtc]$_2$	0.1	0.1142	9.151 x 10^{-4}	29.94
		0.01	0..1254	1.004 x 10^{-3}	23.07
		0.001	0.1345	1.077 x 10^{-3}	17.48
H_2SO_4	Blank	1	0.474	3.798 x 10^{-3}	-
	Ni[BuMedtc]$_2$	0.1	0.426	3.413 x 10^{-3}	10.26
		0.01	0.445	3.576 x 10^{-3}	6.05
		0.001	0.459	3.678 x 10^{-3}	3.16

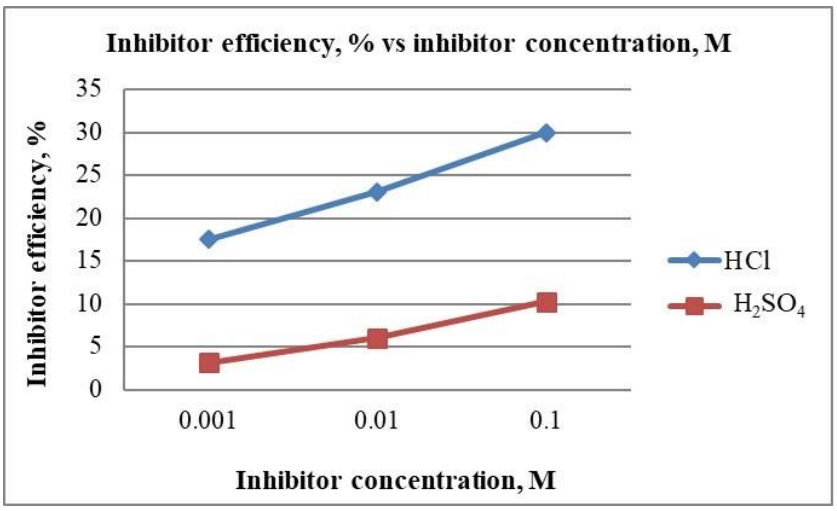

Figure 7. Inhibitor efficiency versus inhibitor concentration in 1M HCl and 1M H_2SO_4

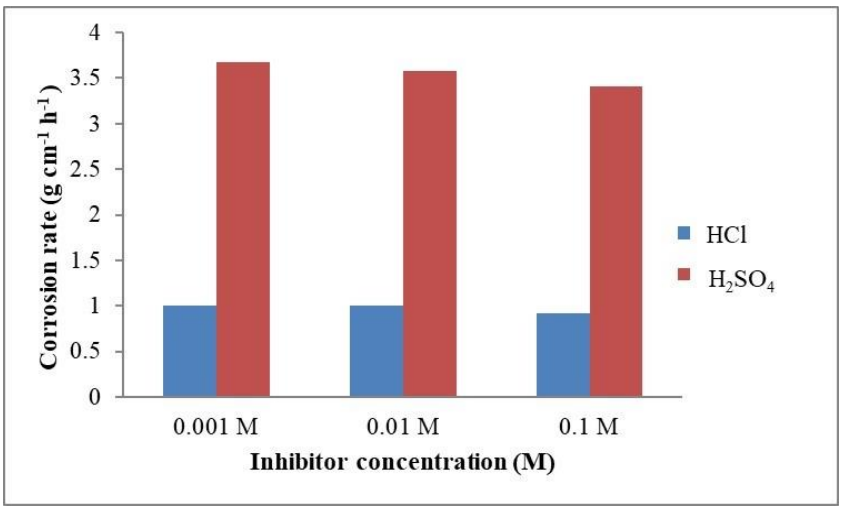

Figure 8. Inhibitor concentration versus corrosion rate in Ni[BuMedtc]$_2$

IV. CONCLUSION

As a conclusion, Ni[BuMedtc]$_2$ was successfully synthesised by in-situ method and characterised by using FTIR-ATR, UV-Vis, elemental analysis and X-ray single diffraction. The crystal structure of Ni[BuMedtc]$_2$ complex adopted a distorted tetrahedral geometry which was the structure of the synthesised Ni[BuMedtc]$_2$ complex and revealed that the coordination made in the complex was S, S-bidentate coordination. The IR spectra were fully parallel with the X-ray single-crystal diffraction. The chemical properties, such as the energy of complex formation, ionisation energy and electron affinity of the Ni[BuMedtc]$_2$ complex, were successfully calculated by using DFT approach. The theoretical data was aligned to the experimental data, proving that the Ni[BuMedtc]$_2$ complex effectively acted as a corrosion inhibitor in this study. The complex demonstrated a promising anti-corrosion activity since the corrosion rate decreased as the inhibitor concentration increased. Finally, Ni[BuMedtc]$_2$ is a good corrosion inhibitor in 1 M HCl but not 1 M H_2SO_4 because H_2SO_4 is a more corrosive acid due to the excessive presence of H^+.

V. ACKNOWLEDGEMENT

This work was supported by the research grant from the Ministry of Higher Education with the grant number of FRGS/1/2016/STG01/UITM/03/6. We are grateful to everyone involved in this project. We wish to express our gratitude to the Faculty of Applied Sciences, Universiti Teknologi MARA (UiTM) Negeri Sembilan Branch, Kuala Pilah Campus, Negeri Sembilan Darul Khusus, Malaysia and the Centre of Research and Instrumentation Management (CRIM), Universiti Kebangsaan Malaysia, Selangor Darul Ehsan, Malaysia for providing the facilities used in this work.

VI. REFERENCES

Andrew, FP & Ajibade, PA 2018, 'Metal complexes of alkyl-aryl dithiocarbamates: Structural studies, anticancer potentials and applications as precursors for semiconductor nanocrystals', Journal of Molecular Structure, vol. 1155, pp. 843-855.

Antonio, ECV, Mayura, MMR, Lucas, FDS, Laercio, Z, Arthur, BDP, Silvana, G, Rafael, ACS & Javier, E 2020, 'New Allyldithiocarbimates: Synthesis, structure and antifungal activity against Phakopsora pachyrhizi and Hemileia vastatrix', Journal of Brazilian Chemical Society, vol. 31, no. 4, pp. 703-715.

Awang, N, Baba, I, Mohd Yousof, NSA & Kamaludin, NF 2010, 'Synthesis and characterization of organotin(IV) *N*-benzyl-*N*-isopropyldithiocarbamate compounds: Cytotoxic assay on human hepatocarcinoma cells (HepG2)', American Journal of Applied Sciences, vol. 7, no. 8, pp. 1047–1052.

Awang, N, Baba, I & Yamin, BM 2011, 'Synthesis, characterization and crystal structure of triphenyltin(IV) *N*-alkyl-*N*-cyclohexyldithiocarbamate compounds', World Applied Sciences Journal, vol. 12, no. 5, pp. 630–635.

Beyramabadi, SA, Morsali, A & Vahidi, SH 2012, 'DFT characterization of 1-acetylpiperazinyl-dithiocarbamate ligand and its transition metal complexes', Journal of Structural Chemistry, vol. 53, no. 4, pp. 665-675.

Bobinihi, FF, Osuntokun, J & Onwudiwe, DC 2018, 'Syntheses and characterization of nickel(II) dithiocarbamate complexes containing NiS4 and NiS2PN moieties: Nickel sulphide nanoparticles from a single source precursor', Journal of Saudi Chemical Society, vol. 22, no. 4, pp. 381-395.

El-Sayed, AE, A, El-Sawaf, Ayman, KE & Metwally, M 2019, 'Synthesis, crystal structure, spectral and thermal investigations of morpholinyldithiocarbamate complexes: A novel coordinated precursor for efficient metal oxide nanophotocatalysts', Inorganica Chimica Acta, vol. 487, pp. 307-315.

Hagen, MVD & Jarnberg, J 2009, Sulphuric, hydrochloric, nitric and phosphoric acids, The Nordic Expert Group for Criteria Documentation of Health Risks from Chemicals, Arbete och Hälsa (report), vol. 43, no. 7, pp. 1-129.

Hebbar, N, Praveen, BM, Prasanna, BM, Venkatesha, TV & Abd Hamid, SB 2014, 'Anthranilic Acid as corrosion inhibitor for mild steel in hydrochloric acid media', Procedia Materials Science, vol. 5, pp. 712–718.

Hong-bo, F, Hui-long, W, Xing-peng, G & Jia-shen, Z 2002, 'Corrosion inhibition mechanism of carbon steel by sodium *N,N*-diethyl dithiocarbamate in hydrochloric acid solution', Anti-Corrosion Methods and Materials, vol. 49, no. 4, pp. 270–276.

Kamaludin, NF, Awang, N, Baba, I, Hamid, A & Meng, CK 2013, 'Synthesis, characterization and crystal structure of organotin(IV) *N*-Butyl-*N*-phenyldithiocarbamate compounds and their cytotoxicity in human leukemia cell lines', Pakistan Journal of Biological Sciences, vol. 16, no.m1, pp. 12-21.

Kanchi, S, Singh, P & Bisetty, K 2014, 'Dithiocarbamates as hazardous remediation agent: A critical review on progress in environmental chemistry for inorganic species studies of 20th century', Arabian Journal of Chemistry, vol. 7, no. 1, pp. 11–25.

Keter, FK, Guzei, IA, Nell, M, Zyl, WEV & Darkwa, J 2014, 'Phosphinogold(I) dithiocarbamate complexes: effect of the nature of phosphine ligand on anticancer properties', Inorganic Chemistry, vol. 53, no. 4, pp. 2058-2067.

Latif, NSH, Ghazali, SAISM, Abdullah, EN, Lahuri, AH, Ngatiman, MF & Dzulkifli, NN 2018, 'Synthesis, structural, density functional theory, and X-ray diffraction study of Zn(II) *N*-Isopropylbenzyldithiocarbamate: anti-corrosion screening in acid media', Indonesia Journal of Chemistry, vol. 18, no. 4, pp. 755-765.

Liu, W, Duan, H, Wei, D, Cui, B & Wang X 2019, 'Stability of diethyl dithiocarbamate chelates with Cu(II), Zn(II) and Mn(II)', Journal of Molecular Structure, vol. 1184, pp. 375-381.

Nabipour, H, Ghammamy, S, Ashuri, S & Aghbolagh, S 2010, 'Synthesis of a new dithiocarbamate compound and study of its biological properties', Journal of Organic Chemistry, vol. 2, pp. 75–80.

Noor Khadijah, MSM, Mustafa, K & Adibatul, H 2014, 'Synthesis, characterization and corrosion inhibition studies of o, m, p-decanoyl thiourea derivatives on mild steel in 0.1 M H_2SO_4 solutions', The Malaysian Journal of Analytical Sciences, vol. 18, no. 1, pp. 21-27.

Onwudiwe, DC, Nthwane, YB, Ekennia, AC & Hosten, E 2016, 'Synthesis, characterization and antimicrobial properties of some mixed ligand complexes of Zn(II) dithiocarbamate with different *N*-donor ligands', Inorganica Chimica Acta, vol. 447, pp. 134–141.

Parveen, M, Mobin, M & Zehra, S, 2016, 'Evaluation of L-tyrosine mixed with sodium dodecylsulphate or cetyl pyridinium chloride as a corrosion inhibitor for mild steel in 1 M HCl: experimental and theoretical studies', RSC Advances, vol. 6, pp. 61235-61248.

Qiang, Y, Zhang, S, Tan, B & Chen, S 2018, 'Evaluation of Ginkgo leaf extract as an eco-friendly corrosion inhibitor of X70 steel in HCl solution', Corrosion Science, vol. 133 no. 6, pp. 1-11.

Samina, M, Karim, A & Venkatachalam, A 2011, 'Corrosion study of iron and copper metals and brass alloy in different medium', E-Journal of Chemistry, vol. 8, no. S1, pp. 344-349.

Sathiyaraj, E, Thirumaran, S, Selvanayagam, S, Sridhar, B & Ciattini, S 2018, 'C-H···Ni and C-H···π(chelate) interactions in nickel(II) complexes involving functionalized dithiocarbamates and triphenylphosphine', Journal of Molecular Structure, vol. 1159, pp. 156-166.

Shetty, SD & Shetty, P 2008, 'Inhibition of mild steel corrosion in acid media by *N*-benzyl-*N*-phenyl thiourea', Indian Journal of Chemical Technology, vol. 15, no. 3, pp. 216–220.

Soltani, N, Salavati, H, Rasouli, N, Paziresh, M & Moghadasi, A 2016, 'Adsorption and corrosion inhibition effect of schiff base ligands on low carbon steel corrosion in hydrochloric acid solution', Chemical Engineering Communications, vol. 203, no. 6, pp. 840-854.

Szolar, OHJ 2007, 'Environmental and pharmaceutical analysis of dithiocarbamates', Analytica Chimica Acta, vol. 582, no. 2, pp. 191–200.